Journal of Soils and Sediments (2026) 26:54
https://doi.org/10.1007/s11368-026-04266-0

SOIL DEGRADATION CONTROL, REMEDIATION AND RECLAMATION

The amelioration effect and mechanism of Calcium-Iron modified Biochar on coastal Saline-Alkali soil

Xueqing Li[1] · Kangfu Sun[1] · Tingting Yang[2] · Jingguo Cao[1] · Li Wu[2] · Aijun Zheng[3] · Shengguo Jiang[2] · Wenjie Zhao[1]

Received: 16 October 2025 / Accepted: 5 February 2026

Abstract

Purpose This study aimed to address the urgent need for coastal saline-alkali soil remediation (critical for agricultural productivity and ecosystem stability) by developing calcium-iron enhanced biochars and evaluating their reclamation efficacy, focusing on structural optimization and salinity reduction mechanisms.

Materials and methods Three calcium-iron modified biochars (BC1, BC2, BC3) were synthesized. Their structural/chemical properties were characterized, followed by 60-day soil incubation with 0.5-2% biochar additions. Soil pH, electrical conductivity, salinity, and sodium adsorption ratio (SAR) were measured, with response surface modeling to optimize BC1 application conditions.

Results and discussion BC1 showed 91.03% higher specific surface area and 58.78% larger pore volume (enriched with C-O, Fe-O, Ca-O groups). At 70% moisture, BC1 significantly outperformed BC2/BC3 ($P<0.05$), reducing salinity by 52.21–71.01% and SAR by 78.51–96.43%. Optimal conditions (2% BC1, 60 days, 70% moisture) achieved 1.14 g/kg salinity (consistent with experimental 1.11 g/kg) via ion exchange/coordination of Na^+, Cl^-, SO_4^{2-}.

Conclusions Calcium-iron modified BC1 is an environmentally sustainable remediation solution, with structural enhancement and ion adsorption mechanisms providing actionable insights for coastal saline-alkali soil reclamation in field applications.

Keywords Calcium-iron modified biochar · Coastal soil reclamation · Saline–alkali soil remediation · Response surface design · Amelioration mechanism

1 Introduction

Soil salinization has emerged as a major global soil degradation issue in recent decades. It currently affects approximately 1 billion ha worldwide, which represents approximately 7% of the total global land area and 20% of all arable land (Zhang et al. 2020b). Owing to variations in climatic conditions, the natural environment, and pedogenic processes, saline-alkali soils exhibit considerable heterogeneity across different regional and national contexts. In China, four primary saline-alkali soil types are recognized based on their geographic distribution: coastal tidal zones, Huang-Huai-Hai alluvial plain, northwestern desert/desert-steppe regions, and northern grassland ecosystems (Yuan et al. 2023). Among these, coastal saline-alkali soils, as a predominant saline soil type in China, are primarily distributed in Liaoning, Hebei, Tianjin, Jiangsu, and Shandong provinces. These soils are characterized by elevated salt content and chloride-type salinization (Zhang and Zhang 2020).Prolonged salinization disrupts the physicochemical structure,

Responsible editor: Remigio Paradelo Núñez

✉ Tingting Yang
yangtt210@126.com

✉ Jingguo Cao
cjg@tust.edu.cn

[1] College of Chemical Engineering and Materials Science, Tianjin University of Science & Technology, No.9, Thirteenth Street, Binhai New Area Economic and Technological Development Zone, Tianjin 300457, China

[2] Tianjin North China Geological Exploration Bureau, No. 67 Guangrui West Road, Hedong District, Tianjin 300170, China

[3] Tianjin Agricultural Development Service Center, No. 5 Xiyuan Road, Hexi District, Tianjin 300061, China

Published online: 17 February 2026

impairs microbial communities, and degrades the biological properties of soils. Excessive salt accumulation in the soil damages the cellular structures of crops and inhibits the uptake of essential nutrient ions via osmotic and ionic stress, thereby severely affecting crop growth and yield (Hailu and Mehari 2021; Meena et al. 2022; Wang et al. 2023). Consequently, the amendment of saline-alkali land is a critical priority for sustainable agriculture.

Biochar has been widely investigated as a soil amendment in recent years owing to its environmental friendliness, cost-effectiveness, and widespread availability. It via adsorption or exchange with Ca^{2+} and Mg^{2+} on its surface, thereby mitigating soil salinity. Biochar, with its nutrient-dense composition, can boost soil fertility by increasing soil organic carbon, total nitrogen, available phosphorus, and available potassium levels, thereby effectively promoting plant growth (Cui et al. 2021; Gao et al. 2024). Despite these advantages, unmodified biochar's drawbacks necessitate targeted modifications. Various modification strategies have been explored to optimize the physicochemical properties of biochar and enhance its remediation efficacy in alleviating saline-alkali soil. For instance, acid-modified biochar can enhance the cation exchange capacity by decreasing its pH and enlarging the specific surface area, thereby reducing soil soluble salt content (Sadegh-Zadeh et al. 2018). However, its long-term stability in soil application is compromised by degradation or decomposition (Sahin et al. 2017). Ethanol-modified biochar exhibits an improved Na^+ adsorption capacity; however, it faces application challenges linked to high production costs, complex processing, and limited long-term stability (Medyńska-Juraszek et al. 2021). Red phosphorus-loaded biochar enhances the specific surface area and reduces the electrical conductivity (EC), salt content, and pH of coastal saline-alkali soil. Nevertheless, it is prone to red phosphorus oxidation and lacks stability (Zhang et al. 2022).

Given the limitations of these approaches, metal modification has emerged as a promising material optimization strategy in saline-alkali land remediation owing to its superior structural stability and adsorption performance. It is primarily used to regulate the soil pH, reduce salinity, and enhance the soil structure. Currently, biochar modified with magnesium oxide, gypsum, aluminum oxides, iron oxides, and calcium oxides can reduce soil pH, EC, and salt content by 1–2%, 28–67%, and 30–65%, respectively (Shan et al. 2022; Wang et al. 2024a). Among these, iron- and calcium-modified biochar offer unique advantages in saline-alkali soil remediation because of their low cost, environmental safety, and effective amelioration performance. Iron-based biochar and calcium-based biochar can reduce soil salinity, pH value and SAR, but their application is limited by unstable iron redox and calcium ion leaching (Chen et al. 2024; Wang et al. 2023; Xu et al. 2023; Zhang et al. 2024a). Calcium-iron composite-modified biochar exhibits better remediation performance than single-modified biochar, with proven effectiveness in related fields such as wastewater treatment and heavy-metal-contaminated soil remediation (Ou et al. 2023; Zhou et al. 2025), though its application and mechanistic research in saline-alkali soil remediation remain insufficient. Most existing studies on saline-alkali soil remediation focus on single-modified biochar with inadequate exploration of dual-metal composite biochar, rarely targeting coastal chloride-type saline-alkali soils with high Na^+ and Cl^- contents (Wang et al. 2024b). Moreover, research on key application parameters (e.g., biochar dosage, soil water content), remediation mechanism, and cost-effectiveness has not received adequate attention (Campion et al. 2023).

Response surface methodology (RSM) is a multivariate optimization technique that primarily analyzes the relationships between process parameters using statistical and mathematical models, thereby enabling process optimization with minimal experimental trials(Behera et al. 2018). For instance, a four-factor optimization model for urea-phosphate-potassium (UPK) synthesis—incorporating temperature, KCl ratio, reaction time, and phosphoric acid concentration—demonstrated high reliability, with predicted and actual yields closely aligned (69.8% versus $67.58 \pm 1.25\%$) (Yang et al. 2020). In agricultural production, RSM has been employed to construct a multi-factor synergistic optimization model for irrigation volume, nitrogen fertilization rate, and substrate addition rate, thereby providing a scientific basis for water fertilizer management in corn cultivation (Emran et al. 2024). It has also been applied to optimize tartaric acid-mediated soil remediation, ultimately removing 89.35% of the zinc contamination. The method shows considerable promise for the remediation of heavy metal contamination in soil (Alman-Abad et al. 2020).

In this study, we employed RSM to optimize key parameters for materials used to amend saline-alkali soils. Specifically, we aimed to identify optimal experimental conditions, reduce testing duration, enhance remediation efficacy, and promote the practical application of these materials. We prepared CaFe-BC and investigated their remediation efficacy and underlying mechanisms in coastal saline-alkali soil by integrating RSM with comprehensive material characterization. The main research objectives were as follows: (1) CaFe-BC materials with varying Fe and Ca loadings were synthesized. Subsequently, the influence of different modification techniques on the biochar structures was explored by analyzing the

microstructural features, chemical compositions, and properties of the loaded elements. (2) A soil cultivation experiment was conducted to assess the effectiveness of CaFe-BC for remediating soil salinity. This included evaluating its effect on the overall salt content of the soil and eight specific salt ions (Na^+, Mg^{2+}, Ca^{2+}, K^+, Cl^-, HCO_3^-, CO_3^{2-}, and SO_4^{2-}). RSM was employed to identify the critical factors and optimize the remediation conditions. (3) Fourier-transform infrared spectroscopy (FTIR) and X-ray photoelectron spectroscopy (XPS) were used to characterize CaFe-BC before and after soil cultivation. These analyses attempted to elucidate the microscale reaction mechanisms between CaFe-BC and salt ions and provide insights into the interaction of the material with the soil environment. These findings provide scientific justification and technical support for the remediation of saline–alkali soils and promotion of sustainable agricultural development.

2 Materials and methods

2.1 Test soil and reagents

Soil samples were collected from a 0–20 cm farmland stratum in Xiaowangzhuang Town, Binhai New Area, Tianjin. Following collection, the soil was subjected to natural air drying and passed through a 2-mm sieve prior to experimentation. The soil attributes were as follows: pH (8.13 ± 0.05), EC (3,470.00 ± 19.29) μS/cm, and organic matter content (7.45 ± 0.28 g/kg). The water-soluble cation contents were as follows: K^+ (0.035 ± 0.005 g/kg), Na^+ (1.310 ± 0.025 g/kg), Ca^{2+} (0.585 ± 0.008 g/kg), Mg^{2+} (0.386 ± 0.007 g/kg). The water-soluble anion concentrations were as follows: HCO_3^- (0.150 ± 0.010 g/kg), Cl^- (0.900 ± 0.021 g/kg), SO_4^{2-} (0.465 ± 0.015 g/kg). The total water-soluble salt content was 3.83 ± 0.04 g/kg.

The modification utilized analytical-grade reagents, including $Fe(NO_3)_3$, $CaSO_4 \cdot 2\ H_2O$, and HCl, all sourced from Jiangtian Chemical Co., Ltd (China).

2.2 Preparation of biochar and calcium-iron composite-modified Biochar

2.2.1 Biomass

The corn stover biomass was sequentially cleaned with municipal tap water and purified deionized water, with each procedure performed in triplicate. Subsequent processing involved dehydration at 80 °C in a drying oven, mechanical pulverization with an electric mill, and particle size standardization via 60-mesh sieving.

2.2.2 Biochar

A 10.00 g aliquot of preprocessed corn stover was subjected to controlled pyrolysis in a quartz tube reactor. Continuous N_2 flow was maintained while the temperature increased at a rate of 5 °C per min until it reached 350 °C. This was followed by a 120-min isothermal retention period to produce the base biochar material (BC).

2.2.3 Calcium-iron composite-modified biochar

Iron(III)-containing modification reagents can improve biochar structure and enhance its catalytic activity by reducing reaction energy barriers, promoting electron transfer, optimizing pore structure, and providing adsorption active sites (Zeng et al. 2022). And $CaSO_4$-modified biochar could reduce soil salinity through the exchange reaction between loaded Ca^{2+} and Na^+ (Zhang et al. 2025). Therefore, Fe-Ca composite biochar was prepared in this study to investigate its structural characteristics and performance in saline-alkali land remediation.

$Fe(NO_3)_3$ and $CaSO_4 \cdot 2\ H_2O$ were precisely weighed according to predefined mass ratios, dissolved in 500 mL of deionized water, and mixed with biomass at specified ratios. The mixture was continuously stirred until it reached a homogeneous state, followed by a pH adjustment to 3.00 ± 0.05 using 1 mol/L hydrochloric acid (Dalahmeh et al. 2020). The homogeneous suspension was subjected to ultrasonic treatment (25 °C, 2 h), followed by mechanical agitation with a six-position magnetic stirrer (300 rpm, 2 h). The resulting solids were collected through vacuum filtration and dehydrated at 80 °C. The subsequent pyrolysis in a tubular reactor was conducted with temperature programming (at a ramp rate of 5 °C/min to 350 °C) followed by a 120-min isothermal period, resulting in the formation of the CaFe-BC. The mass ratios of Fe to Ca to biomass were set as 0.25:0.5:10, 0. 5:0.5:10, and 0.75:0.5:10, respectively. The calcium-iron composite modified biochar prepared under these conditions were designated as BC1, BC2, and BC3.

2.3 Soil static cultivation experiment

A total of 200 g of the test saline-alkali soil was precisely weighed. Amendments BC, BC1, BC2, and BC3 were incorporated into the soil at mass ratios of 0.5%, 1%, and 2%, respectively, and thoroughly mixed. A blank control group (CK) was also established without the addition of any biochar. The homogenized soil was transferred to polyethylene bottles (8.5 cm diameter × 14 cm depth) for static cultivation experiments, with three field moisture-holding capacity levels (70%, 50%, and 30%) established to simulate soil improvement under different water management scenarios.

Each treatment was conducted in triplicate. Soil sampling for parameter measurements was conducted on days 10, 30, and 60 of the incubation period.

2.4 Response surface experiment

RSM was utilized to examine the effects of three factors—field water-holding capacity, biochar addition ratio, and soil incubation time—on total soil salinity. A three-factor, three-level experimental design was formulated using Design Expert 12.0 software, adhering to the Box-Behnken design (BBD) principle, with soil salinity reduction as the response variable. The details of the experimental design are presented in Tables S1 and S2 in the Appendix.

2.5 Batch adsorption experiment

A mixed solution was prepared to contain Na^+ (500 mg/L), Ca^{2+} (200 mg/L), Mg^{2+} (100 mg/L), K^+ (100 mg/L) Cl^- (300 mg/L), SO_4^{2-} (150 mg/L), and HCO_3^- (50 mg/L). The pH was adjusted to 8.00 using HCl to mimic the key characteristics of coastal surface irrigation water. Subsequently, 100 mL of this solution was transferred to a conical flask, and 1.0000 g of BC, BC1, BC2, and BC3 was added individually. The flasks were incubated in a constant-temperature shaker at 25 °C for 24 h. Following incubation, the supernatant was collected to analyze the salt ion concentration in the water.

2.6 Characterization and detection methods

The elemental composition of the biochar, including organic carbon, hydrogen, nitrogen, and oxygen, was measured using an elemental analyzer (EA, UNICUBE, Germany) (Wu et al. 2022). The ash content was determined using the mass difference method following combustion at 750 °C for 2 h (Jabeen et al. 2020). The porous characteristics of the biochar materials, including their specific surface areas and pore size distributions, were determined by nitrogen physisorption measurements conducted with an automated surface area analyzer (BSD-660 M A6B6M, China) (Huang et al. 2022). The morphological structure and surface features of the biochar were analyzed using scanning electron microscopy (SEM; XL30E, FEI, USA). FTIR (TENSOR27, Germany) was used to characterize the surface functional groups of the biochar (Das et al. 2021). X-ray photoelectron spectroscopy (XPS; Thermo Scientific ESCALAB 250XI, USA) was used to analyze the surface elemental composition and functional groups. The crystal structure of the biochar was investigated using XRD (Shimadzu, Japan). The crystal particle size was calculated using the Scherrer formula. The detailed characterization methods and calculation methods are outlined in Text S1 of the Appendix.

The pH values of the soil and biochar were determined using a pH meter (PHS-2 C, Mettler-Toledo Instrument Co., Ltd.) at a soil-to-water ratio of 1:5. Soil EC was measured by preparing a 1:5 soil-water extraction solution, thoroughly shaking it to reach equilibrium, and measuring the value using a calibrated digital conductivity meter (DDS-11 A, Shanghai Yidi Scientific Instrument Co., Ltd., China). The residue-drying method was used to quantify the water-soluble total salt content of the soil. The soil organic matter content was measured using potassium dichromate oxidation via the heating method (Osman et al. 2013). Soil water-soluble ions (K^+, Na^+, Ca^{2+}, Mg^{2+}, SO_4^{2-}, and Cl^-) were analyzed using an ion chromatograph (PIC-10, Qingdao Purun Instrument Co., Ltd.), while CO_3^{2-} and HCO_3^- were quantified via the double indicator neutralization titration method (Yu-yan et al. 2020). The SAR, a critical parameter reflecting the exchange capacity of sodium ions with calcium and magnesium ions in the soil, was calculated using the following formula (Qadir et al. 2021):

$$SAR = N\alpha^+ / \sqrt{\frac{(Ca^2 + Mg^{2+})}{2}} \tag{1}$$

The concentrations of Na^+, Ca^{2+}, Mg^{2+}, and K^+ in the aqueous solution were determined using an ion chromatograph (PIC-10, Qingdao Purun Instrument Co., Ltd., China). The adsorption capacity (Q, mg/g) and removal efficiency (R, %) of the materials for these ions were calculated using Eqs. (2) and (3):

$$Q = \frac{V(C_0 - C_1)}{m} \tag{2}$$

$$R = \frac{C_0 - C_1}{C_0} \times 100\% \tag{3}$$

where C_0 (mg/L) is the initial concentrations of Na^+, Ca^{2+}, Mg^{2+}, and K^+ in the solution; C_1 (mg/L) is their concentrations post-adsorption; V (L) is the solution volume; and m (g) is the mass of the material.

2.7 Statistical analysis methods

Data processing and analysis were conducted using Excel 2010, and graphing was performed with Origin 2021. One-way ANOVA was applied via SPSS 23.0 to evaluate significant differences, with statistical significance defined as $P<0.05$; multiple comparisons were further carried out using Tukey's HSD test. All experiments and measurements were performed in triplicate.

3 Results and discussion

3.1 Structural characteristics of biochar and calcium-iron composite-modified biochar

3.1.1 Physicochemical characteristics of biochar

The surface morphologies of the BC and CaFe-BCs are illustrated in Fig. 1. After pyrolysis, BC retained a tubular structure similar to that of straw, featuring a smooth surface and an abundant porous architecture. BC1, BC2, and BC3 maintained their original bundle-like structures while exhibiting distinct surface porosities characterized by rough and wrinkled textures. Specific surface area analysis (detailed in Table 1) revealed that the specific surface areas of BC1, BC2, and BC3 were 10.14-fold, 8.19-fold, and 8.77-fold higher than that of BC, respectively. Concurrently, their pore volumes increased by 1.43-fold, 0.28-fold, and 0.54-fold relative to that of BC, respectively (Wang et al. 2024c). As shown in Table 1, the predominant element in both the BC and modified biochar was carbon, with concentrations ranging from 50.14% to 65.51%. Compared with BC, the carbon content of the three modified samples (BC1, BC2, and BC3) decreased, whereas the oxygen content increased. Notably, BC1 displayed the highest oxygen content (15.46%), indicating that the calcium-iron modification facilitated the development of oxygen-containing functional groups. This enhancement contributed to its improved hydrophilicity and polarity (Wang et al. 2015). Furthermore, the iron content in BC1, BC2, and BC3 ranged from 1.98% to 5.02%, while the calcium content ranged from 8.90% to 10.35%. These results confirmed the successful loading of iron and calcium onto the biochar surface. The elemental contents varied among materials owing to different calcium-iron modification reagent ratios, with BC3 exhibiting the highest iron content (5.02%) and BC1 showing the highest calcium content (10.35%).

3.1.2 XRD analysis

XRD was employed to characterize the effect of modification on the crystal structure of the biochar. For the raw biochar (BC) shown in Fig. 2(a), distinct diffraction peaks were observed at $2\theta = 36°$ and 43.3°. These peaks corresponded to carbon diffraction patterns, signifying the presence of graphitic carbon in the biochar (Qin et al. 2022). In the modified biochars (BC1, BC2, and BC3), peaks at 34.1° and 45.5° corresponded to Fe_2O_3 diffraction patterns (Murphin Kumar et al. 2021), while the 35.5° peak was associated with Fe_3O_4 (Yoon et al. 2017), thereby confirming the reaction of iron with biochar during modification to produce iron oxide crystals. All modified samples displayed distinct peaks at $2\theta = 29.6°$ and 55.8°, which were attributed to the (104) plane of $CaCO_3$ (calcite) (Hussein et al. 2020), thereby indicating the presence of calcium as $CaCO_3$ on the biochar surface. Notably, the modified biochars exhibited additional peaks at $2\theta = 20.9°$, 26.6°, 36.5°, 39.5°, and 42.4°, corresponding to the (220), (130), (121), (420), and (321) planes of $CaFe_2O_4$ (Xiang et al. 2024b), respectively, indicating the presence of $CaFe_2O_4$. These findings align with those of Xin

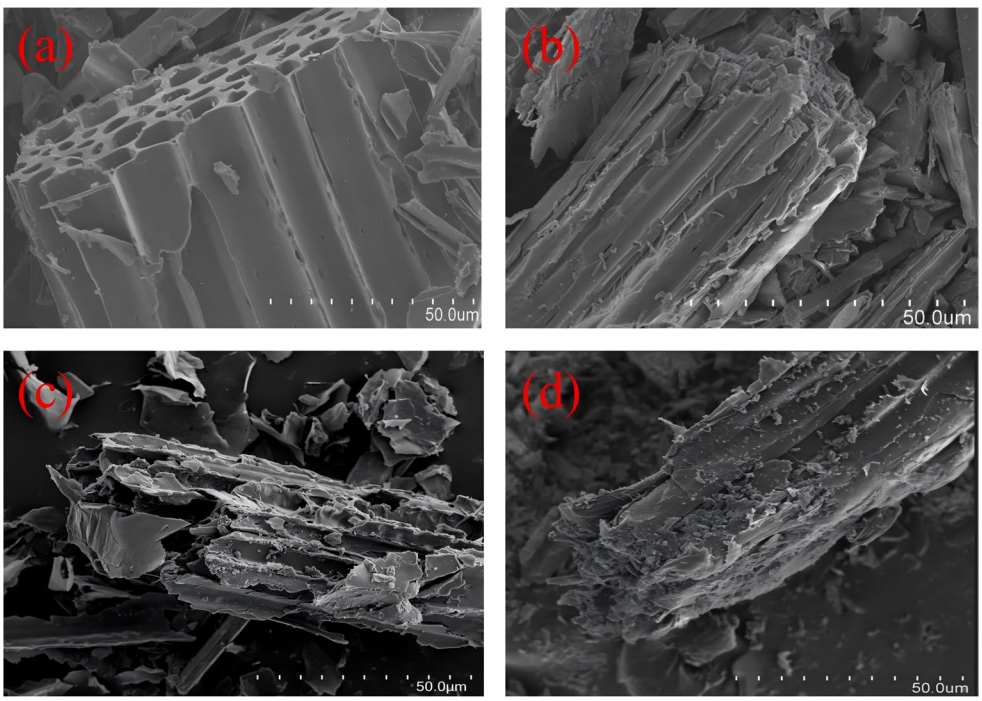

Fig. 1 Scanning Electron Microscope images of Biochar (**a**), Calcium-iron modified biochar (Fe: Ca: biomass mass ratio of 0.25:0.5:10) (**b**), Calcium-iron modified biochar (Fe: Ca: biomass mass ratio of 0.5:0.5:10) (**c**), Calcium-iron modified biochar (Fe: Ca: biomass mass ratio of 0.75:0.5:10) (**d**)

Table 1 Physical and chemical properties of Biochar and modified Biochar

Types of biochar	pH	C content(%)	H content(%)	O content(%)	*N* content(%)	Fe content(%)	Ca content(%)	Specific surface area(m^2/g)	Total pore volume(cm^3/g)	Micro-pore volume (cm^3/g)	Meso-pore volume (cm^3/g)	Macropore volume (cm^3/g)	Aper-ture (nm)	Ash (%)
BC	8.27 ±0.15a	65.51 ±0.22a	3.93 ±0.07a	14.27 ±0.12a	1.66 ±0.09a	-	-	11.59 ±0.10c	0.054 ±0.010c	0.008± 0.001b	0.036± 0.002c	0.010± 0.001a	6.88 ±0.10a	44.15 ±0.84a
BC1	5.25 ±0.06b	51.15 ±0.24b	1.61 ±0.09b	15.46 ±0.24a	1.35 ±0.09b	2.70 ±0.19b	10.35 ±0.07a	129.16 ±1.56a	0.131 ±0.010a	0.015± 0.002a	0.102± 0.003a	0.014 ± 0.001a	4.05 ±0.07b	32.17 ±0.74c
BC2	5.64 ±0.08b	56.27 ±0.19c	1.58 ±0.08b	14.38 ±0.16a	1.36 ±0.06b	1.98 ±0.13c	7.89 ±0.13b	106.53 ±1.57b	0.069 ±0.009b	0.011± 0.001b	0.045± 0.002b	0.013± 0.001a	5.73 ±0.15c	36.78 ±1.11b
BC3	5.50 ±0.10b	50.14 ±0.15b	2.49 ±0.11c	15.13 ±0.18a	1.76 ±0.09a	5.02 ±0.10a	6.90 ±0.15c	113.18 ±1.23b	0.083 ±0.003b	0.013± 0.001b	0.058 ±0.002b	0.012± 0.002b	5.12 ±0.09d	39.15 ±0.72b

et al.(Xiang et al. 2024b), who reported $CaFe_2O_4$ formation following modification with $Fe(NO_3)_3$ and $CaCl_2$. Calculations using the Scherrer formula (Table S3) demonstrate its precision for quantitative analysis of biochar crystal particle size. As the iron-to-calcium loading ratio increases, the particle sizes of Fe_2O_3, Fe_3O_4, and $CaFe_2O_4$ crystals exhibited a decreasing trend: In BC3, the Fe_3O_4 particle size (25.3 nm) decreased by 11.5% compared to BC1 (28.6 nm), while the $CaFe_2O_4$ particle size (24.1 nm) decreased by 9.9% compared to BC1 (26.8 nm). This may result from the high Fe loading promoting crystal nucleation rates exceeding growth rates, leading to finer microcrystals—a pattern previously confirmed in studies of Fe/Ca composite oxide-modified biochar(Hu et al. 2024). Meanwhile, $CaCO_3$ exhibited the smallest particle size (20.8 nm) in BC3, likely due to excess Fe^{3+} inhibiting $CaCO_3$ crystal aggregation, consistent with findings on Fe ion regulation of calcium carbonate crystallization behavior (Liu et al. 2025). However, as indicated by the adsorption experiments discussed, BC1 exhibits superior overall adsorption performance compared to BC3 due to the synergistic effect of its optimal pore structure and crystal distribution.

3.1.3 FTIR analysis

As illustrated in Fig. 2(b), the FTIR spectra characterized the functional group features of the four types of biochar. The four biochar samples (BC, BC1, BC2, and BC3) displayed absorption peaks at 3450 cm^{-1}, 2925 cm^{-1}, 1543 cm^{-1}, 1071 cm^{-1}, and 788 cm^{-1}, respectively. These peaks were attributed to -OH, $-CH_3$, -C=C/C=O, C-O-C, and -CH vibrations, respectively (Ahmed et al. 2016). Compared to BC, BC1, BC2, and BC3 exhibited significantly enhanced C-O-C and -OH peaks, indicating that the metal composite modification increased the number of oxygenated functional groups in the material (Wu et al. 2020). The -OH peak was the strongest in BC1. Additionally, Fe-O and Ca-O vibrational peaks were observed at 570 and 698 cm^{-1} in the three modified biochars (Dumitru et al. 2013; Jung KyungWon et al. 2016), thereby confirming the successful incorporation of Fe and Ca into the biochar structure (di Bitonto et al. 2020). Quantitative analysis of FTIR characteristic peak areas (Table S4) reveals that calcium-iron modification significantly increases the surface oxygen-containing functional groups and metal-oxygen bond peak areas of biochar: the -OH peak area (2154) in BC1 increased by 67.5% compared to the original BC (1286), while the C-O-C peak area (1863) in BC1 increased by 95.7% compared to BC (952). This indicates that the modification promotes the formation of oxygen-containing functional groups such as hydroxyl and ether bonds by introducing Fe and Ca elements, thereby enhancing the material's hydrophilicity and ion-binding

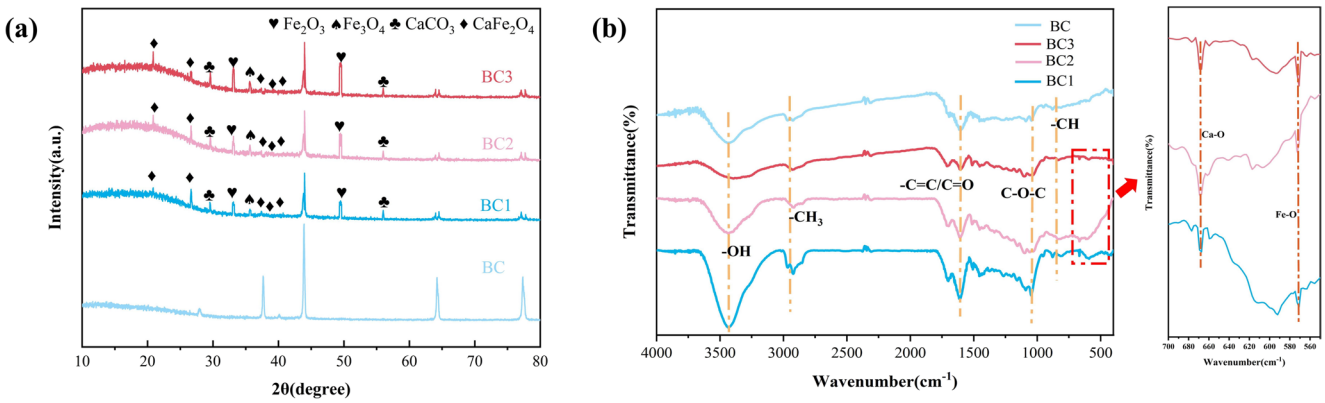

Fig. 2 X-ray Diffraction and Fourier Transform Infrared Spectroscopy patterns of biochar and modified biochar, (**a**) XRD, (**b**) FTIR

capacity (Hu et al. 2024). Regarding metal-oxygen bonds, the Fe-O peak area (896) in BC1 increased by 37.4% and 14.1% compared to BC2 (652) and BC3 (785), respectively. The Ca-O peak area (752) increased by 27.7% and 10.9% compared to BC2 (589) and BC3 (678) by 27.7% and 10.9%, respectively. This correlates with BC1's highest Ca loading (10.35%, Table 1), further validating successful Ca and Fe loading and confirming BC1 possesses the richest metal-oxygen active sites on its surface.

3.1.4 XPS analysis

In the C1s spectrum presented in Fig. 3(a), the central peaks at 284.80 eV, 286.32 eV, and 288.34 eV were assigned to the C-C, C-O, and C=O bonds, respectively (Yao 2024). In contrast to BC, the C-O content in BC1, BC2, and BC3 increased from 18.12% to 23.35%, 21.19%, and 22.07%, respectively, whereas the C=O content increased from 10.57% to 14.62%, 13.77%, and 13.31%, respectively. This finding suggests that the CaFe-BC modification altered the distribution of the oxygen-containing functional groups in the biochar (Zhuo et al. 2022). In the O1s spectrum (Fig. 3(b), the three peaks in biochar and modified biochar corresponded to metal-oxygen functional groups (M-O), surface-anchored metal hydroxide groups (M-OH), and carbon-bonded hydroxyl groups (C-OH) in biochar(Liang et al. 2017). Compared to BC, BC1, BC2, and BC3 showed increased M-O and M-OH contents and decreased C-OH content due to the introduction of additional reagents during modification (Chen et al. 2021). In the Fe 2p spectrum (Fig. 3(c), the Fe 2p3/2 and Fe 2p1/2 components were detected at 710.90 eV and 726.80 eV in BC1, BC2, and BC3, signifying the presence of iron in both Fe(II) and Fe(III) valence states (Xiang et al. 2024a). Quantitative analysis revealed Fe(II) contents of 35.28%, 37.32%, and 39.59% and Fe(III) contents of 38.55%, 39.17%, and 39.28% in BC1, BC2, and BC3, respectively, thereby corroborating the XRD characterization results of Fe_2O_3 and Fe_3O_4. In the Ca 2p spectrum (Fig. 3(d), peaks at 347.73 eV and 351.59 eV in the modified samples corresponded to Ca 2p3/2 and Ca 2p1/2 of Ca-O, likely resulting from calcium ion-hydroxyl radical complex formation during pyrolysis (Pan et al. 2024). The relative Ca-O bonds in BC1, BC2, and BC3 were considerably higher the Ca-O-C bonds, primarily because of high-temperature conditions that disrupted Ca-O-C bonds, releasing free Ca^{2+} ions to interact with oxygen radicals and increased Ca-O bond content (Liu et al. 2022).

3.2 Influence of biochar and calcium-iron composite-modified biochar on soil physicochemical properties

3.2.1 Impact of biochar versus calcium-iron composite-modified biochar on soil pH values

The effects of adding BC and modified biochar (BC1, BC2, and BC3) on soil pH are presented in Fig. 4(a). On cultivation days 10, 30, and 60, the soil pH in the modified biochar treatments decreased significantly, with a continuous downward trend as the cultivation period increased. By day 60, soil pH values in the BC, BC1, BC2, and BC3 treatments decreased to 7.53–7.74, 7.23–7.61, 7.41–7.72, and 7.36–7.63, respectively—representing 1.40–3.21% decreases from day 10 ($P<0.05$). At field moisture contents of 30%, 50%, and 70%, the soil pH further decreased with increasing moisture, with the most notable decrease (1.16–7.07% reduction) observed at 70% moisture. Among the treatments, BC1 exhibited the greatest pH-reducing effect by day 60 at 70% moisture, reducing the soil pH to 7.47, 7.33, and 7.23 at addition rates of 0.5%, 1%, and 2%, respectively. This was 2.86–3.98% lower than that of BC ($P<0.05$). This indicates that BC1 had the strongest neutralizing effect on soil pH at elevated moisture levels and application rates.

All biochar treatments (BC, BC1, BC2, and BC3) showed the ability to decrease soil pH. Among them, BC1, BC2, and BC3 demonstrated considerable alkalinity reduction,

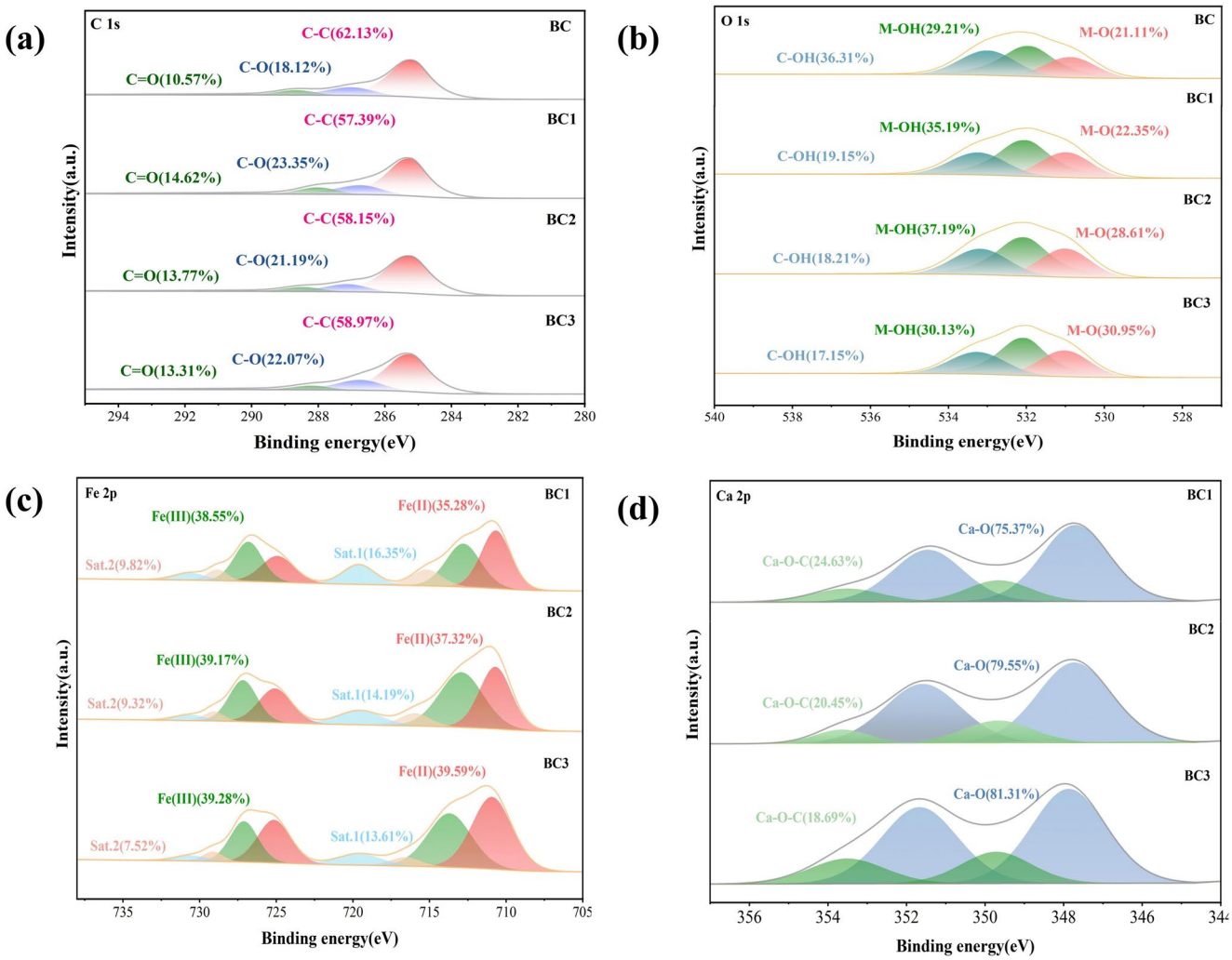

Fig. 3 X-ray Photoelectron Spectroscopy spectra of biochar and modified biochar, (**a**) C1s, (**b**) O1s, (**c**) Fe2p, (**d**) Ca2p

resulting from two mechanisms: (1) The pH of the three modified biochars ranged from 5.25 to 5.64. When applied to the soil, the soil pH was lowered via acid-base neutralization. BC1 (pH 5.25), exhibiting a pH lower than that of BC2 (5.64) and BC3 (5.50), effectively neutralized the soil hydroxide ions, causing a marked decrease in pH(Zhang et al. 2020a). (2) Ca^{2+} loaded on BC1–BC3 underwent ion exchange with soil Na^{+}, reducing sodium salts (e.g., NaCl, Na_2SO_4) and generating calcium salts (e.g., $CaCl_2$, $CaSO_4$) with weaker alkalinity, thereby mitigating sodium-induced alkalinity (Zhao et al. 2018). BC1 showed the most pronounced pH-lowering effect, likely due to its high calcium content (10.35%).

3.2.2 Impact of biochar and calcium-iron composite-modified biochar on soil electrical conductivity

Figure 4(b) illustrates that the BC and modified biochars (BC1, BC2, and BC3) substantially influenced soil EC. As cultivation time increased, soil EC values across all treatment groups decreased, reaching their lowest levels by day 60, with reduction rates of 56.35–75.98% (BC), 62.55–88.17% (BC1), 58.04–81.85% (BC2), and 60.60–81.41.60.41% (BC3) ($P<0.05$). At field moisture contents of 30%, 50%, and 70%, soil EC further decreased with increasing moisture and reached its minimum at 70% (reduction rates of 12.25–87.14%), thereby indicating that higher moisture enhances the salinity improvement efficiency of the materials. By day 60, at 70% moisture and a 2% application rate, BC1 reduced soil EC by 88.17% ($P<0.05$), outperforming previously reported amendments(Table S5), such as lithium slag (60.53%)(Zhang et al. 2024b), vinegar residue (60.83%)(Zhao et al. 2020b), sludge (55.83%)(Zhao et al. 2020b), and earthworm compost (50.03%). This superiority stems from the following: (1) The larger specific surface area (129.16 m^2/g) and more abundant pores of BC1 provided more active sites for soil improvement (Saifullah et al. 2018); (2) Adequate moisture facilitated salt ion

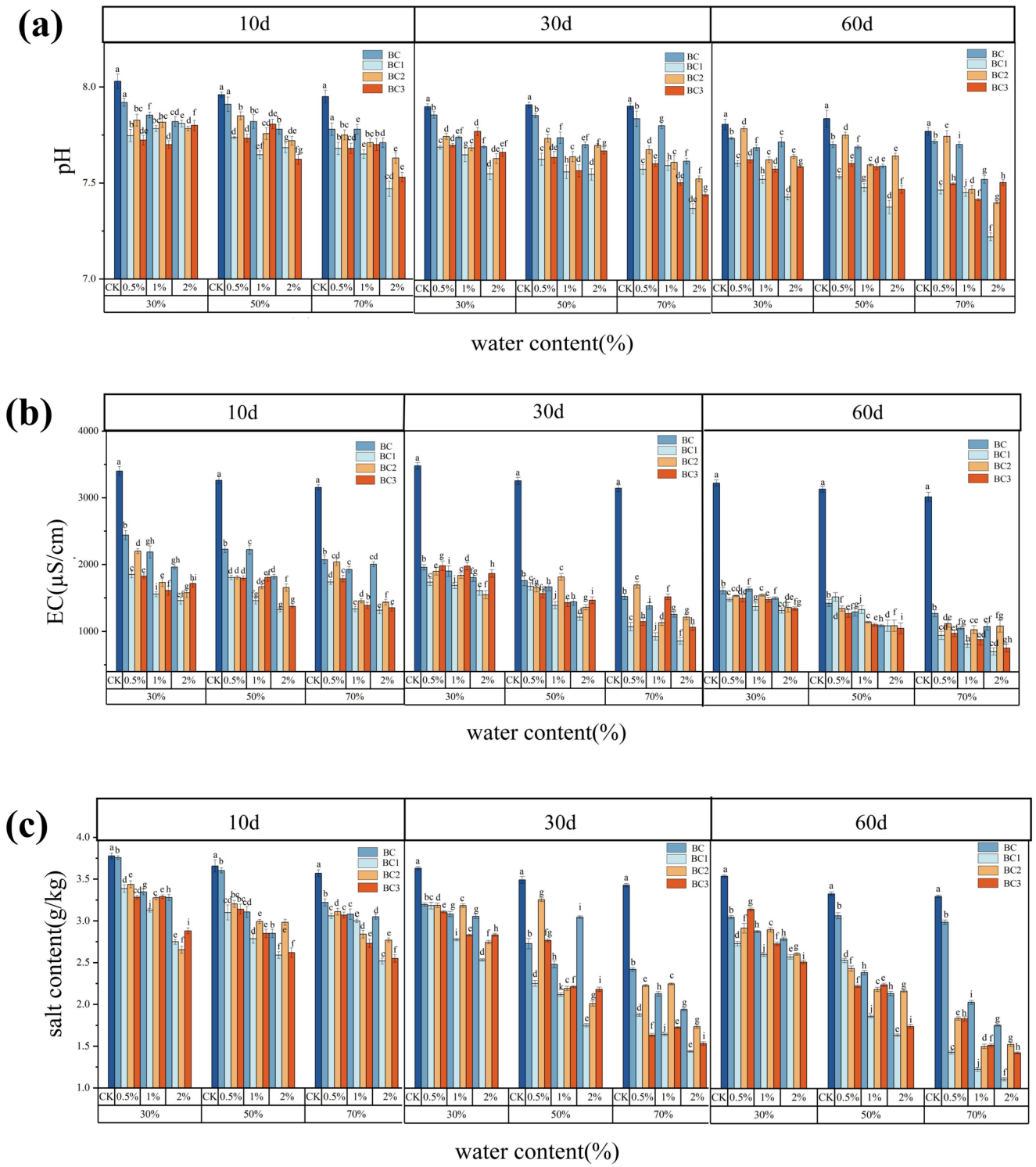

Fig. 4 Effects of adding 0.5%, 1%, and 2% biochar and modified biochar on soil pH (**a**), electrical conductivity (**b**), and salinity (**c**) under field moisture content conditions of 30%, 50%, and 70%

migration and enhanced mass transfer between ions and the amendment (Zhao et al. 2019).

3.3 Impact of biochar and calcium-iron composite-modified biochar on soil salinity

The effects of the BC and modified biochars (BC1, BC2, and BC3) on soil salinity amelioration are shown in Fig. 4(c). On cultivation days 10, 30, and 60, soil salinity in the modified biochar treatments decreased significantly, and the reduction became more pronounced over time. By day 60, soil salinity in the BC, BC1, BC2, and BC3 treatments decreased by 20.26–53.95%, 28.42–71.01%, 23.68–60.00.68.00%, and 25.53–62.63%, respectively. These reductions were 1.37–5.70% greater than those observed on day 10 ($P<0.05$). At field moisture contents of 30%, 50%, and 70%, soil salinity further decreased with increasing moisture, peaking at 70% moisture (53.95–71.01% reduction). At 70% moisture and 60-day cultivation, the 2% BC1 application reduced soil salinity to 1.11 g/kg, which represented a 71.01% decrease from that of the CK group ($P<0.05$), thereby demonstrating the optimal salinity amelioration of BC1 under high moisture and application rates. The decreases in soil salinity caused by BC1, BC2, and BC3 can be attributed to the presence of abundant oxygen-containing functional groups and well-developed pore structures, which promote the adsorption of soluble cations, such as Na^+. These findings align with those reported by Wei et al. (Zhao et al. 2020a), who reported a decrease in soil pH and salinity when corn straw biochar was used (Table S5). The 71.01% salinity reduction of BC1 outperformed cow manure/chicken manure-gypsum (48.70%) (Andrade Foronda and Colinet 2022), humic acid (45.18%)(Zhao et al. 2025), and fly ash (38.95%) (Zhou et al. 2024) (Table S5), thereby highlighting its superior potential for saline-alkali soil remediation.

3.4 Impact of Biochar versus calcium-iron composite-modified Biochar on water-soluble base ion content

Figure 5(a)-(g) illustrates the effects of the BC and modified biochars on soil water-soluble ions. In the 3D visualization, the x- and y-axes denote the moisture content and cultivation time, respectively, while the z-axis represents variations in soil water-soluble ion concentrations. Colored spheres, sized according to ion content, depict various treatment groups. As shown, all treatments effectively decreased soil Na^+, Cl^-, and SO_4^{2-} concentrations while increasing soil Ca^{2+}, Mg^{2+}, and K^+ levels. After 60 days, BC1 showed optimal performance: under 70% moisture, Treatment with 2% BC1 significantly reduced the contents of Na^+, Cl^-, and SO_4^{2-} in the soil by 98.18%, 97.77%, and 97.55%, respectively, compared with CK ($P<0.05$), while increasing Ca^{2+}, Mg^{2+}, and K^+ by 29.42%, 15.54%, and 69.57% ($P<0.05$), respectively. This can be attributed to the coordination of the surface oxygen-containing groups (-COOH, -OH) of BC with Na^+ and the absorption of anions via electrostatic interactions, thereby decreasing Na^+, Cl^-, and SO_4^{2-} concentrations (Sánchez et al. 2022).

Figure 5(h) illustrates the effect of the BC and modified biochars on the soil SAR after 60 days of soil cultivation under different field moisture contents. SAR values decreased in soils treated with BC, BC1, BC2, and BC3. At 70% field moisture content, the SAR values in the BC, BC1, BC2, and BC3 treatments decreased by 78.51–96.43% relative to 30% moisture. Among them, 2% BC1 application decreased the soil SAR to a minimum of 0.02. Wei et al (Wu et al. 2024). reported similar findings, with a decrease in the SAR following straw biochar application. The reduction in soil SAR by CaFe-BC can be attributed to ion exchange between divalent cations (Ca^{2+}, Mg^{2+}) on biochar surfaces and Na^+ in soil colloids, thereby reducing Na^+ adsorbed on colloid surfaces(Tsai et al. 2012). BC1 had the highest specific surface area and abundant oxygen-containing functional groups, thereby demonstrating a more pronounced SAR reduction effect.

3.5 Adsorption of salt ions in water by Biochar and calcium-iron composite-modified biochar

To elucidate the intrinsic mechanisms by which materials reduce soil salinity, this study systematically investigated the adsorption performance of biochar and modified biochar toward cations (Na^+, Ca^{2+}, Mg^{2+}, K^+) and anions (Cl^-, SO_4^{2-}, HCO_3^-) in aqueous solutions. The adsorption results for relevant ions are shown in Fig. 6(a)-(b) and Fig. S2., respectively. All three modified biochar materials effectively adsorbed the aforementioned ions, though their adsorption capacities exhibited significant differences. BC1 adsorbed Na^+, Mg^{2+}, Ca^{2+}, and K^+ at concentrations of 65.42 mg/g, 35.19 mg/g, 45.12 mg/g, and 21.13 mg/g, respectively. For anions, the adsorption capacities were 58.26 mg/g for Cl^-, 42.35 mg/g for SO_4^{2-}, and 18.79 mg/g for HCO_3^-. Overall, BC1 demonstrated significantly superior adsorption performance compared to BC2 and BC3. This advantage of BC1 is primarily attributed to its larger specific surface area (129.16 m^2/g) and abundant oxygen-containing functional groups (-OH、C-O-C). These structural characteristics provide more sites for ion adsorption and enable BC1 to exhibit distinct selective adsorption properties toward target ions. In multi-ion coexisting systems, it preferentially adsorbs Na^+ and Cl^-, with BC1 demonstrating the most outstanding adsorption performance for Na^+ among all target ions (Fig. 6(a). This phenomenon is primarily attributed to Na^+'s

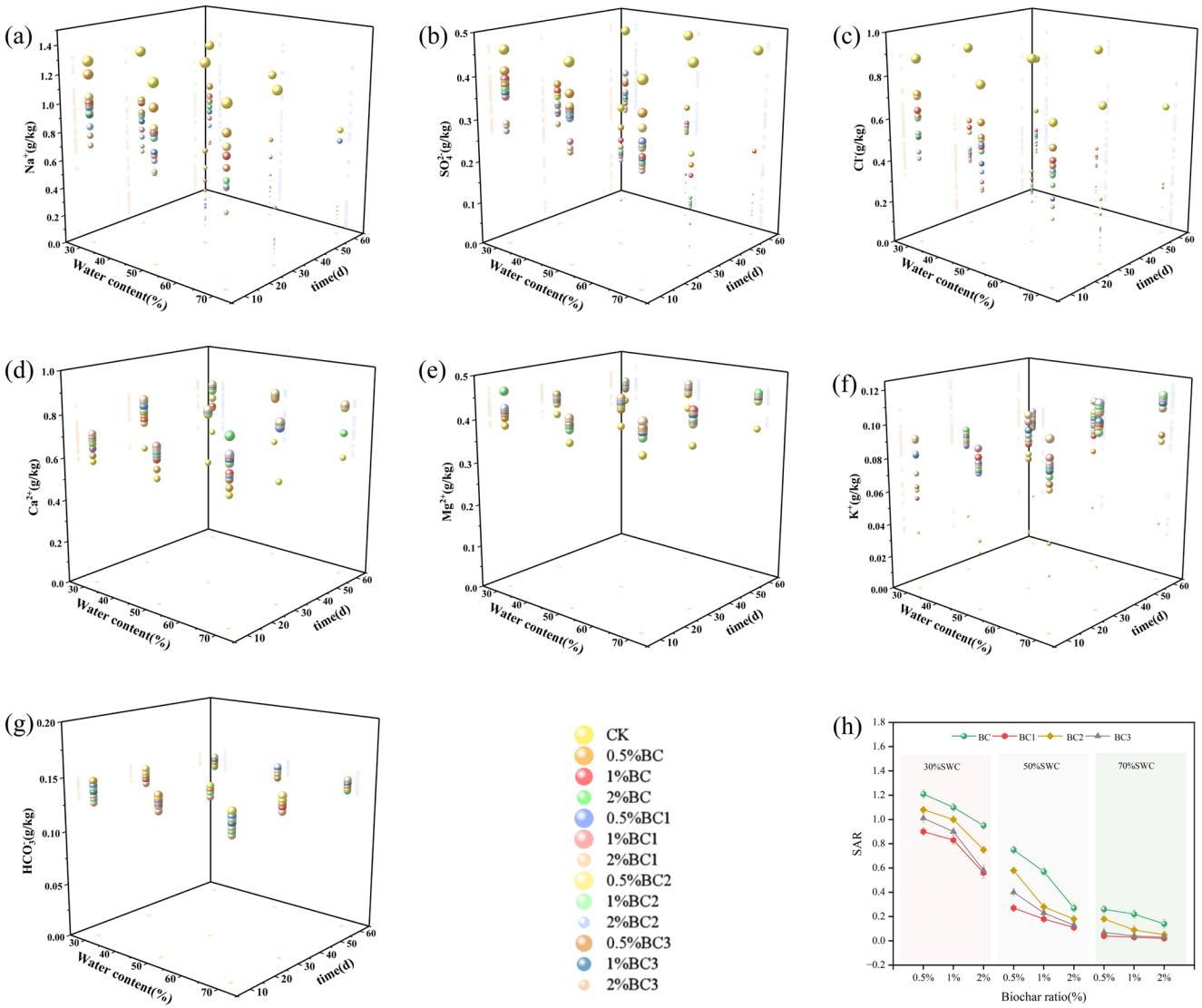

Fig. 5 Under field moisture content conditions of 30%, 50%, and 70%, the effects of adding 0.5%, 1%, and 2% biochar and modified biochar on soil water-soluble Na^+ (**a**), SO_4^{2-} (**b**), Cl^- (**c**), Ca^{2+} (**d**), Mg^{2+} (**e**), K^+ (**f**), HCO_3^- (**g**), and soil sodium adsorption ratio (**h**)

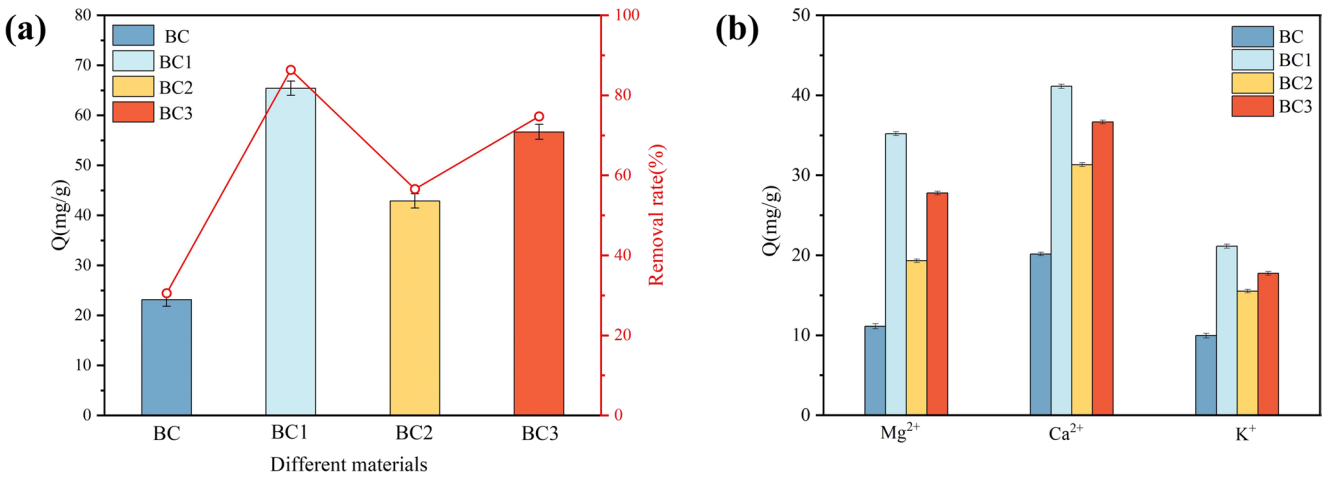

Fig. 6 Adsorption capacity of biochar and modified biochar for (**a**) Na^+ and (**b**) Mg^{2+}, Ca^{2+}, and K^+ in water

lower hydration energy (−406 kJ/mol), faster migration rate, specific binding affinity with oxygen-containing functional groups, and smaller ionic radius (0.095 nm). These properties facilitate easier entry into the biochar's pore structure for adsorption and immobilization(Tu et al. 2021).

3.6 Response surface experiment

The effects of three factors—field water-holding capacity, biochar amendment rate, and soil incubation time—on total soil salinity were examined using Design Expert 13 software (Table 2). The experimental data were analyzed via quadratic multiple regression to derive the quadratic regression equation, as shown in Eq. (4):

$$Y = 1.98 - 0.1174A - 0.3352B - 0.2434C \\ -0.024AB + 0.0075AC - 0.0461BC \\ +0.5020A^2 + 0.1109B^2 + 0.0878C^2 \quad (4)$$

where, A, B, C, and Y are the moisture content (%), cultivation time (d), biochar proportion (%), and salt content (g/kg), respectively.

As illustrated in Table 2, the ANOVA showed that the response surface regression model was highly significant ($P<0.0001$), validating its accuracy in predicting the experimental data (Fig. 7(a)). The model presented a coefficient of determination (R^2) of 0.99, an adjusted coefficient of determination (Adj R^2) of 0.98, and a predicted coefficient of determination (Pred R^2) of 0.95, underscoring superior reliability and predictive competence. Factors B, C, and A^2 exhibited extremely significant effects ($P<0.0001$) on soil salinity, while A, B^2, and C^2 had significant effects ($P<0.05$). Based on the F-values, the order of factors influencing soil salinity was cultivation time > biochar application rate > moisture content.

The response surface plots derived from the quadratic regression model enabled an intuitive analysis of the influences of different factors on soil salinity. When one variable is fixed, the interaction between the other two factors is reflected in the slope of the response surface and density of the contour lines; steeper slopes and denser contours indicate more pronounced effects. As shown in Fig. 7(b)–(d), an interaction exists between the cultivation time, biochar application rate, and soil salinity. The model predicted the minimum soil salinity of 1.14 g/kg at 70% moisture content after 60 days of cultivation, with a 2% biochar application. Under these conditions, the measured soil salinity in the cultivation experiment was 1.11 g/kg, with a deviation of 2.63%, demonstrating the high predictive accuracy of the model.

3.7 Mechanistic analysis of calcium-iron composite-modified Biochar for saline-alkali soil improvement

Following soil amelioration, the BC and modified biochars were isolated from the soil, and structural characterization was performed to explore the mechanisms underlying soil salinity reduction. As shown in Fig. 8(a), the FTIR spectra indicated that the composition of functional groups in the modified biochar remained largely consistent before and after soil amelioration despite significant variations in the intensity of the vibration peaks for each functional group. Specifically, in contrast to the unmodified BC, the -OH and -C=C vibration peaks in the modified biochar were notably weakened following soil amelioration, while the C-O-C peak was significantly enhanced. This occurs because Na^+ coordinates with dissociated $-O^-$ to consume hydroxyl groups, interacts with the π electrons of C=C, and promotes hydroxyl condensation to form more ether bonds, thereby indicating that modified biochar fixes Na^+ through

Table 2 Experimental design scheme and results of response surface method

Source	Sum of Squares	df	Mean Square	F-value	*p*-Value	
Model	2.52	9	0.2805	99.81	<0.0001	significant
A-water content	0.1026	1	0.1026	36.52	0.0005	
B-time	0.8546	1	0.8546	304.14	<0.0001	
C-Biochar ratio	0.4651	1	0.4651	165.53	<0.0001	
AB	0.0024	1	0.0024	0.8367	0.3908	
AC	0.0002	1	0.0002	0.0851	0.7789	
BC	0.0091	1	0.0091	3.25	0.1142	
A^2	1.06	1	1.06	377.13	<0.0001	
B^2	0.0468	1	0.0468	16.64	0.0047	
C^2	0.0243	1	0.0243	8.63	0.0218	
Residual	0.0197	7	0.0028			
Lack of Fit	0.0048	3	0.0016	0.4292	0.7435	not significant
Pure Error	0.0149	4	0.0037			
Cor Total	2.54	16				

R^2=0.99 Adjusted R^2=0.98 Predicted R^2=0.95

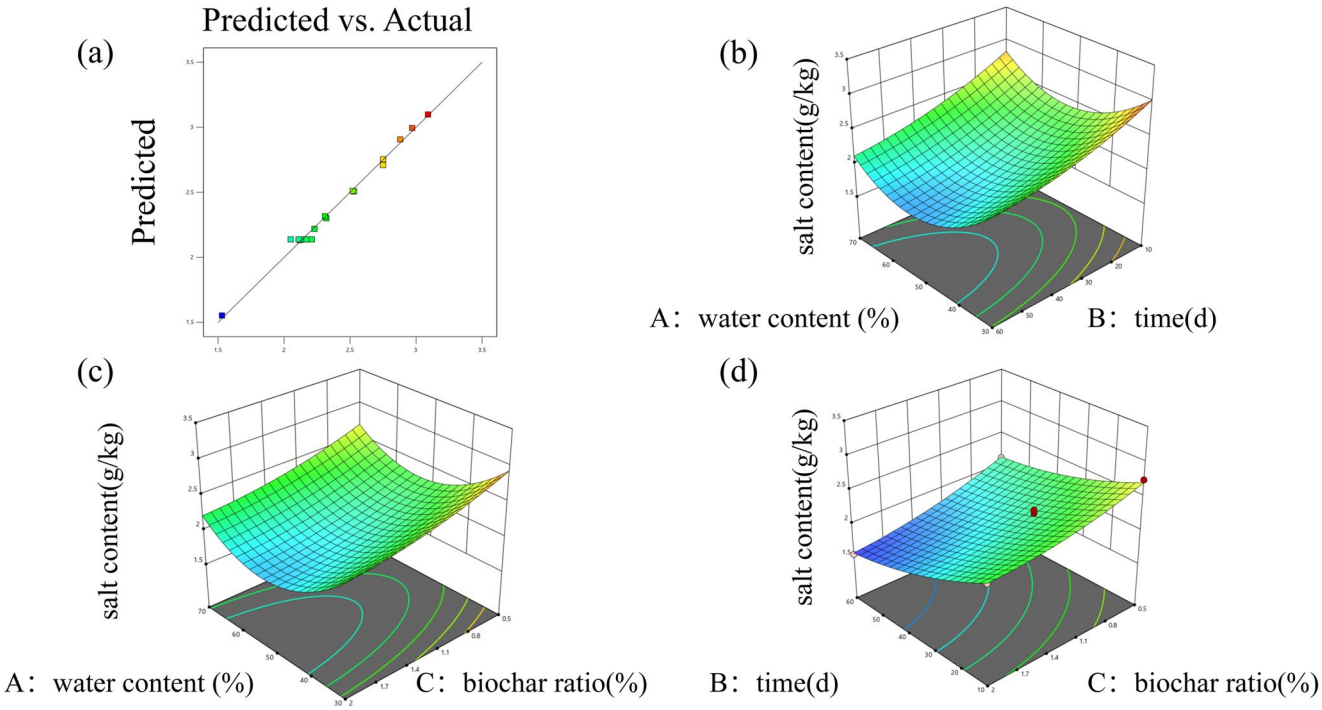

Fig. 7 (**a**) Comparison of response surface predicted values and experimental values; (**b**) Interaction diagram of moisture content and time on soil salinity; (**c**) Interaction diagram of moisture content and biochar addition ratio on soil salinity; (**d**) Interaction diagram of time and biochar addition ratio on soil salinity

functional group alterations(Yang et al. 2024). Additionally, modified biochar demonstrated a substantial amplification of the -CH vibration peak following soil amelioration, likely due to ion exchange with soil Na^+(Guo et al. 2022). Furthermore, the significant enhancement of the Fe-O vibration peak in CaFe-BC suggests that Fe mainly participates in ion exchange via surface hydroxyl groups to fix Na^+. The disappearance of the Ca-O bond may result from Ca reduces soil salinity through ion exchange and precipitation reactions(Li et al. 2023). Moreover, XRD spectra (Fig. 2(a) confirm that $CaCO_3$/$CaFe_2O_4$ loaded on CaFe-BC could enhance ion exchange efficiency by increasing affinity.

Further analysis of the XPS results revealed substantial variations in the elemental valence states of the modified biochars (BC1, BC2, and BC3) before and after soil improvement, with BC1 exhibiting the most considerable difference. The C-C peak of BC1 increased by 9.33% following soil improvement, indicating a carbon reduction. Meanwhile, the contents of C-O and C=O decreased by 10.69% and 12.01%, respectively (Fig. S1), indicating that these oxygen-containing functional groups participated in the adsorption process of soil salt ions and underwent ion exchange reactions with Na^+, Cl^-, and SO_4^{2-} in the soil (Gonçalo Filho et al. 2020). Based on the O1s XPS data presented in Fig. 8(b), the M-OH and M-O contents of BC1 increased after soil cultivation, primarily due to ion exchange reactions between surface hydroxyl groups and soil Na^+(Xue et al. 2024). Additionally, the Ca-O-C content of BC1 decreased from 24.63% to 21.33%, while the Ca-O content increased from 75.37% to 78.67% (Fig. 8(d) after cultivation. Additionally, the Fe(III) content decreased (Fig. 8(c), further indicating that Na^+ participated in ion exchange reactions with the surface hydroxyl groups of iron oxides(Kang et al. 2023).

Soil cultivation and bath adsorption tests showed that BC1 exhibited the best performance in saline-alkali soil amelioration and salt ion adsorption. The characterization of BC1 before and after soil amelioration revealed its primary improvement mechanism, which is attributed to distinctive structural features and elemental composition: (1) In terms of physical structure, the acidic modification environment could dissolve amorphous carbon and ash impurities in the carbon skeleton of biochar through the etching effect of H^+, effectively widening the pore channels and removing pore blockages (Fig. 1 (b)). As a result, BC1 demonstrated the highest specific surface area (129.16 m^2/g) and most well-developed pore structure (pore volume of 0.131 cm^3/g), thereby providing numerous active sites and effective ion transport channels. (2) The acidic modification environment also inhibits the hydrolysis of Fe^{3+} and Ca^{2+}, ensuring that both metal ions are uniformly adsorbed on the biochar surface in an ionic state. This ultimately achieved an optimal loading ratio of Fe (2.70%) and Ca (10.35%), enhancing the performance of the biochar. This improvement is attributed

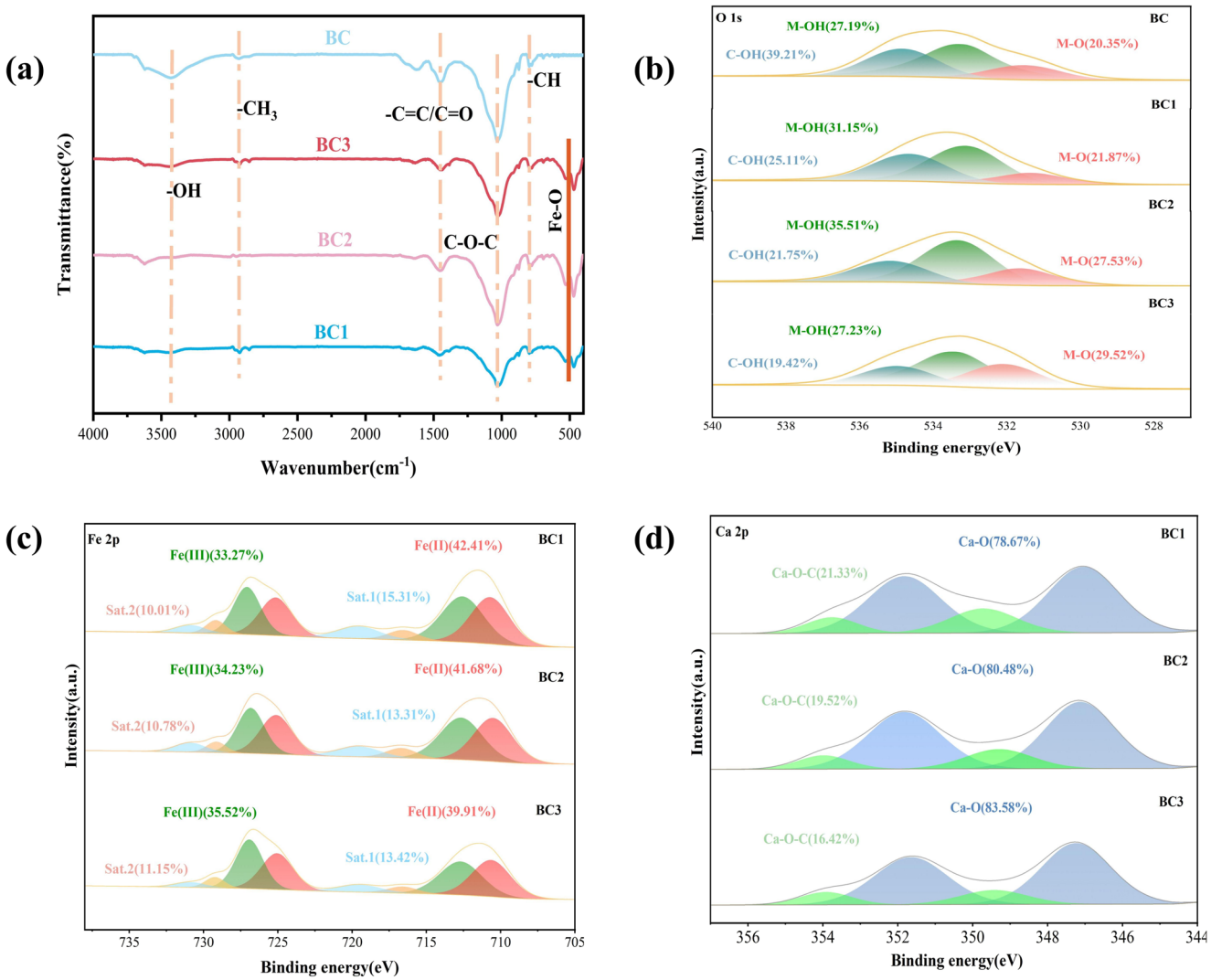

Fig. 8 Fourier Transform Infrared Spectroscopy and X-ray Photoelectron Spectroscopy spectra of biochar and modified biochar soil adsorption, (**a**) FTIR spectrum, (**b**) O1s, (**c**) Fe2p, (**d**) Ca2p

to the loaded Fe and Ca elements optimizing the surface active sites and improving structural stability. In contrast, although BC2 and BC3 exhibited greater specific surface areas; however, excessive Fe/Ca loading caused non-uniform surface properties, resulting in diminished performance of biocahr (Table 1). Therefore, rational control of elemental loading ratios is crucial for optimizing biochar performance.

According to the results presented earlier, the proposed mechanism of CaFe-BC in the remediation of saline-alkali soil is depicted in Fig. 9: (1) Ion Exchange: the Ca (10.35%) loaded on BC1 exchanges with soil Na^+, significantly reducing sodium ion content. Additionally, surface-loaded $CaCO_3$ and $CaFe_2O_4$ offer abundant ion exchange sites for salt ions, thereby amplifying this effect(Fig. 2(a)). (2) Coordination adsorption: the oxygen-rich functional groups (-OH, C-O-C, C-O, and C=O) (Fig. 2(b)) in BC1 promote the formation of stable coordination complexes with Na^+, thereby effectively lowering soil salinity. (3) Electrostatic adsorption: Fe(II) and Fe(III) loaded on BC1 adsorb Cl^- and SO_4^{2-} via electrostatic interactions. (4) Physical adsorption: the highly developed pore structure of BC1 fixes soil salt ions through physical adsorption (Fig. 1(b)). In summary, ion exchange and coordination adsorption are the primary mechanisms by which CaFe-BC ameliorates saline-alkali soils.

3.8 Cost-effectiveness analysis

The synthesis of CaFe-BC takes corn stover, a freely available agricultural waste, as the core raw material, which not only achieves the high-efficiency resource utilization of agricultural solid waste but also significantly reduces the basic cost of substrate preparation. The reagents adopted

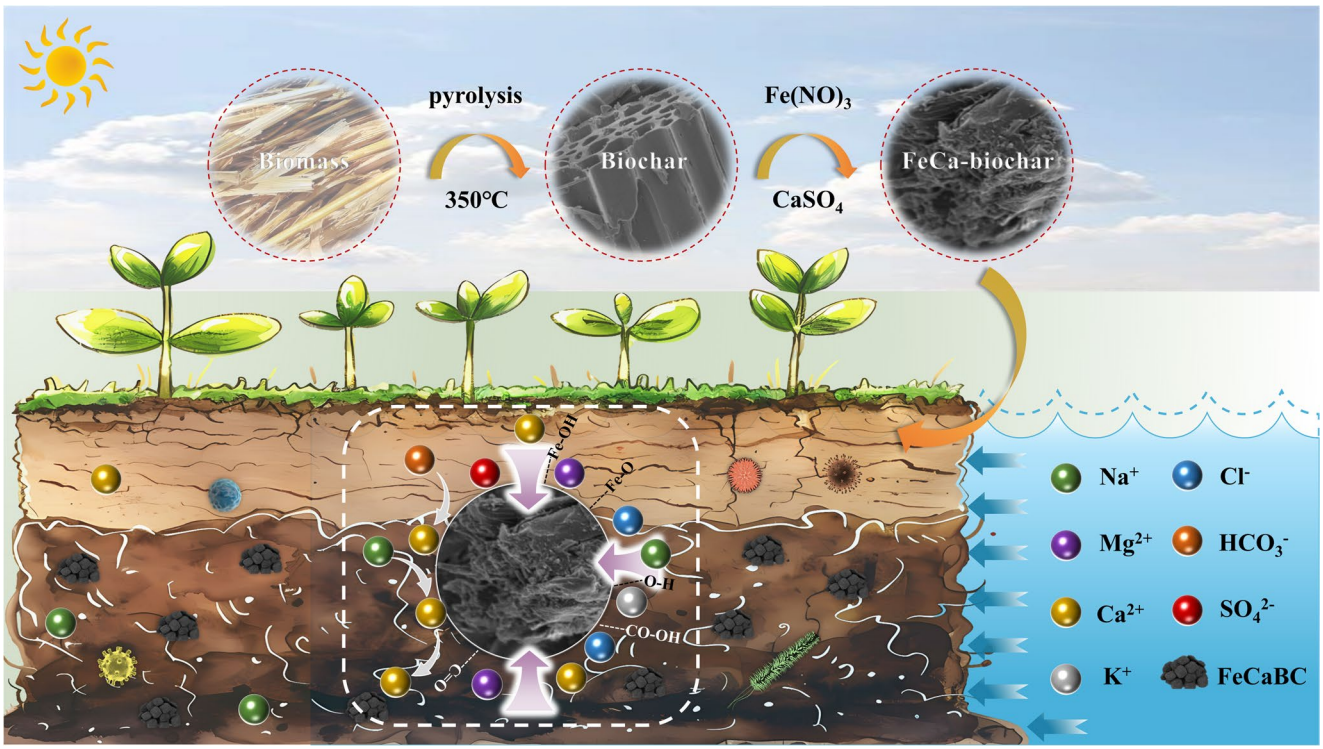

Fig. 9 Adsorption mechanism of calcium-iron composite-modified biochar on saline-alkali soil

in its modification process are $Fe(NO_3)_3 \cdot 9\ H_2O$ and $CaSO_4 \cdot 2\ H_2O$, with market unit prices of 0.041 USD per gram and 0.1605 USD per gram, respectively—both are common, easily accessible, and low-cost reagents in the chemical industry. Based on the 47% yield of biochar, the final preparation cost of per gram of CaFe-BC is merely 0.012 USD. According to existing research reports, the preparation cost of biochar-based functional materials commonly used in the field of environmental remediation generally ranges from 1 USD per gram to 200 USD per gram (Krasucka et al. 2021). The cost of CaFe-BC is reduced by 1–2 orders of magnitude compared with similar materials, demonstrating extremely significant economic advantages. Furthermore, the amelioration effect of calcium-iron modified biochar is significantly higher than that of other amendments (Table S5). This low-cost characteristic stems from the resource recycling of agricultural waste and the rational selection of cheap modification reagents, which not only effectively lowers the economic threshold for large-scale production of the material but also provides solid economic feasibility support for its large-scale promotion and application in practical scenarios such as farmland soil remediation.

4 Conclusion

In this study, three CaFe-BCs (BC1, BC2, and BC3) with different loading ratios were used to analyze the effects of modification on the biochar structure and examine how they improve coastal saline-alkali soils and the underlying mechanisms. The results showed that BC1 had the largest specific surface area, pore volume, and calcium content compared with those observed for BC2 and BC3. In soil incubation experiments, BC1 reduced soil pH, EC, total salinity, SAR, and concentrations of Na^+, Cl^-, and SO_4^{2-} by 11.07%, 88.17%, 71.01%, 96.43%, 98.18%, 97.77%, and 97.55% by day 60, respectively ($P<0.05$). RSM identified the optimal amelioration conditions of 70% soil moisture and 2% BC1 application, under which BC1 demonstrated considerable efficacy. The FTIR, XRD, and XPS analyses of BC1 before and after soil amelioration, demonstrated by its abundant functional groups (-COOH, -OH, -C=O, Fe-OH, and Fe-O), facilitated the effective adsorption of soil salt ions via cation exchange, coordination, and electrostatic and physical adsorption mechanisms, thereby reducing soil salinity and effectively ameliorating coastal saline-alkali soils.

5 Limitations and future research directions

The static cultivation experiments in this study were conducted for 60 days within a controlled sealed system (polyethylene bottles) under fixed moisture content settings (30%, 50%, 70%). Although these conditions differ from the environmental factors encountered in actual field trials—such as rainfall leaching, temperature fluctuations, and plant root activity—the findings of this study provide a foundational basis for application in field trials. In the future, long-term field positioning experiments should be carried out to verify the amelioration effect under real agricultural production conditions, explore the interaction between modified biochar, soil microorganisms, and crops, optimize the biochar modification process parameters. Meanwhile, advanced characterization technologies should be used to deepen the research on the amelioration mechanism at the molecular level, providing more comprehensive technical support and scientific basis for the comprehensive management of coastal saline-alkali soil.

Supplementary information The online version contains supplementary material available at https://doi.org/10.1007/s11368-026-04266-0.

Acknowledgements This research was funded by Tianjin North China Geological Exploration Bureau (HK2024-B03) and Tianjin Metrology Science and Technology Program (2025TJMT014).

Author contributions Xueqing Li: Writing-original draft, Formal analysis, Investigation. Kangfu Sun: Resources, Conceptualization, Supervision. Tingting Yang: Supervision, Writing-review & editing, Project administration. Jingguo Cao: Investigation, Writing-review & editing, Funding acquisition. Li Wu: Validation, Investigation. Aijun Zheng: Validation, Investigation. Shengguo Jiang: Investigation, Validation. Wenjie Zhao: Investigation, Formal analysis.

Data availability Data will be made available on request.

Declarations

Competing interests Authors declare no competing interests.

References

Ahmed MB, Zhou JL, Ngo HH, Guo WS, Chen MF (2016) Progress in the preparation and application of modified biochar for improved contaminant removal from water and wastewater. Bioresour Technol 214:836–851. https://doi.org/10.1016/j.biortech.2016.05.057

Alman-Abad ZS, Pirkharrati H, Asadzadeh F, Maleki-Kakelar M (2020) Application of response surface methodology for optimization of zinc elimination from a polluted soil using tartaric acid. Adsorpt Sci Technol 38:79–93. https://doi.org/10.1177/0263617420916592

Andrade Foronda D, Colinet G (2022) Combined application of organic amendments and gypsum to reclaim saline–alkali soil. Agriculture 12:1049. https://doi.org/10.3390/agriculture12071049

Behera SK, Meena H, Chakraborty S, Meikap BC (2018) Application of response surface methodology (RSM) for optimization of leaching parameters for ash reduction from low-grade coal. Int J Min Sci Technol 28:621–629. https://doi.org/10.1016/j.ijmst.2018.04.014

Campion L, Bekchanova M, Malina R, Kuppens T (2023) The costs and benefits of biochar production and use: a systematic review. J Cleaner Prod 408:137138. https://doi.org/10.1016/j.jclepro.2023.137138

Chen YN, Xu FT, Li H, Li YP, Liu YH, Chen YR, Li ML, Li LSZ, Jiang HJ, Chen L (2021) Simple hydrothermal synthesis of magnetic $MnFe_2O_4$-sludge biochar composites for removal of aqueous Pb^{2+}. J Anal Appl Pyrolysis. https://doi.org/10.1016/j.jaap.2021.105173

Chen M, Wu L, Ding X, Liu L, Li Y, Fei C, Zhang S (2024) Fe-modified biochar improved the stability of soil aggregates and organic carbon: evidence from enzymatic activity and microbial composition. Land Degrad Dev 35:732–743. https://doi.org/10.1002/ldr.4948

Cui Q, Xia JB, Yang HJ, Liu JT, Shao PS (2021) Biochar and effective microorganisms promote *Sesbania cannabina* growth and soil quality in the coastal saline-alkali soil of the Yellow River Delta, China. Sci Total Environ. https://doi.org/10.1016/j.scitotenv.2020.143801

Dalahmeh SS, Stenström Y, Jebrane M, Hylander LD, Daniel G, Heinmaa I (2020) Efficiency of Iron- and Calcium-Impregnated Biochar in adsorbing phosphate from wastewater in onsite wastewater treatment systems. Front Environ Sci 8. https://doi.org/10.3389/fenvs.2020.538539

Das SK, Ghosh GK, Avasthe RK, Sinha K (2021) Compositional heterogeneity of different biochar: effect of pyrolysis temperature and feedstocks. J Environ Manage 278:111501. https://doi.org/10.1016/j.jenvman.2020.111501

di Bitonto L, Reynel-Avila HE, Mendoza-Castillo DI, Bonilla-Petriciolet A, Durán-Valle CJ, Pastore C (2020) Synthesis and characterization of nanostructured calcium oxides supported onto biochar and their application as catalysts for biodiesel production. Renew Energy 160:52–66. https://doi.org/10.1016/j.renene.2020.06.045

Dumitru R, Papa F, Balint I, Culita DC, Munteanu C, Stanica N, Ianculescu A, Diamandescu L, Carp O (2013) Mesoporous cobalt ferrite: a rival of platinum catalyst in methane combustion reaction. Appl Catal A Gen 467:178–186. https://doi.org/10.1016/j.apcata.2013.07.013

Emran M, El-Gamal EH, Haddad AM, Ibrahim OM (2024) Response surface methodology for optimizing water and fertilizer requirements for maize (*Zea mays* L.) growth in sandy soil. J Soil Sci Plant Nutr 24:6349–6364. https://doi.org/10.1007/s42729-024-01973-w

Gao G, Yan L, Tong KQ, Yu HL, Lu M, Wang L, Niu YS (2024) The potential and prospects of modified biochar for comprehensive management of salt-affected soils and plants: a critical review. Sci Total Environ. https://doi.org/10.1016/j.scitotenv.2023.169618

Gonçalo Filho F, da Silva Dias N, Suddarth SRP, Ferreira JFS, Anderson RG, dos Santos Fernandes C, de Lira RB, Neto MF, Cosme CR (2020) Reclaiming tropical saline-sodic soils with gypsum and cow manure. Water 12:57. https://doi.org/10.3390/w12010057

Guo M, Ma X, Han X, Zhang S, Yuan M, Wang B, Li M (2022) Effects of corn stalks biochar amendment and freezing-thawing on the cd adsorption of saline-alkali soil. Soil Sediment Contam 31:925–940. https://doi.org/10.1080/15320383.2021.2024141

Hailu B, Mehari H (2021) Impacts of soil salinity/sodicity on soil-water relations and plant growth in dry land areas: a review. J Nat Sci Res 12:1–10. https://doi.org/10.7176/JNSR/12-3-01

Hu A, Jiang Y, An J, Huang X, Elgarhy AH, Cao H, Liu G (2024) Novel Fe/Ca oxide co-embedded coconut shell biochar for phosphorus recovery from agricultural return flows. RSC Adv 14:27204–27214. https://doi.org/10.1039/d4ra04795h

Huang XY, Niu XJ, Zhang DQ, Li XQ, Li HS, Wang ZY, Lin Z, Fu ML (2022) Fate and mechanistic insights into nanoscale zerovalent iron (nZVI) activation of sludge derived biochar reacted with Cr(VI). J Environ Manage. https://doi.org/10.1016/j.jenvman.2022.115771

Hussein AI, Ab-Ghani Z, Mat ANC, Ab Ghani NA, Husein A, Ab Rahman I (2020) Synthesis and characterization of spherical calcium carbonate nanoparticles derived from cockle shells. Appl Sci -Basel. https://doi.org/10.3390/app10207170

Jabeen S, Gao XP, Altarawneh M, Hayashi J, Zhang MM, Dlugogorski BZ (2020) Analytical procedure for proximate analysis of algal biomass: case study for *spirulina platensis* and *chlorella vulgaris*. Energy Fuels 34:474–482. https://doi.org/10.1021/acs.energyfuels.9b03156

Jung KyungWon JK, Hyun C, Jeong TaeUn JT, Ahn KyuHong AK (2016) Facile synthesis of magnetic biochar/Fe_3O_4 nanocomposites using electro-magnetization technique and its application on the removal of acid orange 7 from aqueous media. Bioresour Technol 220:672–676. https://doi.org/10.1016/j.biortech.2016.09.035

Kang X, Zhang Q, Liu X, Song J, Guo H, Wang L (2023) The interface mechanism of sludge biochar activating persulfate to remove tetracycline: the role of the CO-Fe bridge at the carbon surface. J Clean Prod 384:135514. https://doi.org/10.1016/j.jclepro.2022.135514

Krasucka P, Pan B, Sik Ok Y, Mohan D, Sarkar B, Oleszczuk P (2021) Engineered biochar – a sustainable solution for the removal of antibiotics from water. Chem Eng J 405:126926. https://doi.org/10.1016/j.cej.2020.126926

Li H, Wang B, Siri M, Liu C, Feng C, Shao X, Liu K (2023) Calcium-modified biochar rather than original biochar decreases salinization indexes of saline-alkaline soil. Environ Sci Pollut Res 30:74966–74976. https://doi.org/10.1007/s11356-023-27701-y

Liang J, Li XM, Yu ZG, Zeng GM, Luo Y, Jiang LB, Yang ZX, Qian YY, Wu HP (2017) Amorphous MnO_2 modified biochar derived from aerobically composted swine manure for adsorption of Pb(II) and Cd(II). ACS Sustain Chem Eng 5:5049–5058. https://doi.org/10.1021/acssuschemeng.7b00434

Liu JX, Zhang WJ, Mei M, Wang T, Chen S, Li JP (2022) A Ca-rich biochar derived from food waste digestate with exceptional adsorption capacity for arsenic (III) removal via a cooperative mechanism. Sep Purif Technol 295:121359. https://doi.org/10.1016/j.seppur.2022.121359

Liu J, Zhou J, Sun M, Zhu M, Zhao Y, Xu J, Chen T, Shakouri M, Zheng L, Sui P, Chen Y, Yang J (2025) Iron-tuned depth-dependent P transformation on calcium carbonate coprecipitates: the impact of Fe and P loadings. Environ Sci Technol 59:15151–15158. https://doi.org/10.1021/acs.est.5c01977

Medyńska-Juraszek A, Álvarez ML, Białowiec A, Jerzykiewicz M (2021) Characterization and sodium cations sorption capacity of chemically modified biochars produced from agricultural and forestry wastes. Materials 14:4714. https://doi.org/10.3390/ma14164714

Meena MD, Narjary B, Sheoran P, Jat HS, Joshi PK, Chinchmalatpure AR (2022) Changes in physical and chemical properties of saline soil amended with municipal solid waste compost and chemical fertilizers in a mustard-pearl millet cropping system. Land Degrad Dev 33:1677–1688. https://doi.org/10.1002/ldr.4256

Murphin Kumar PS, Ganesan S, Al-Muhtaseb AH, Al-Haj L, Elancheziyan M, Shobana S, Kumar G (2021) Tropical fruit waste-derived mesoporous rock-like Fe_2O_3/C composite fabricated with amphiphilic surfactant-templating approach showing massive potential for high-tech applications. Int J Energy Res 45:17417–17430. https://doi.org/10.1002/er.6798

Osman KS, Jashimuddin M, Haque SMS, Miah S (2013) Effect of shifting cultivation on soil physical and chemical properties in Bandarban hill district. Bangladesh J Res 24:791–795. https://doi.org/10.1007/s11676-013-0368-3

Ou WJ, Lan X, Guo J, Cai AM, Liu P, Liu N, Liu YY, Lei YT (2023) Preparation of iron/calcium-modified biochar for phosphate removal from industrial wastewater. J Clean Prod. https://doi.org/10.1016/j.jclepro.2022.135468

Pan F, Wei H, Huang YL, Song JQ, Gao MJ, Zhang ZH, Teng RJ, Jing SS (2024) Phosphorus adsorption by calcium chloride-modified buckwheat hulls biochar and the potential application as a fertilizer. J Clean Prod 444:141233. https://doi.org/10.1016/j.jclepro.2024.141233

Qadir M, Sposito G, Smith C, Oster JD (2021) Reassessing irrigation water quality guidelines for sodicity hazard. Agric Water Manag 255:107054. https://doi.org/10.1016/j.agwat.2021.107054

Qin SN, Fan HD, Jia L, Jin Y, Li ZP, Fan BG (2022) Molecular structure analysis and mercury adsorption mechanism of iron-based modified biochar. Energy Fuels 36:3184–3200. https://doi.org/10.1021/acs.energyfuels.1c03832

Sadegh-Zadeh F, Parichehreh M, Jalili B, Bahmanyar MA (2018) Rehabilitation of calcareous saline-sodic soil by means of biochars and acidified biochars. Land Degrad Dev 29:3262–3271. https://doi.org/10.1002/ldr.3079

Sahin O, Taskin M, Kaya E, Atakol O, Emir E, Inal A, Gunes A (2017) Effect of acid modification of biochar on nutrient availability and maize growth in a calcareous soil. Soil Use Manag 33:447–456. https://doi.org/10.1111/sum.12360

Saifullah DS, Naeem A, Rengel Z, Naidu R (2018) Biochar application for the remediation of salt-affected soils: challenges and opportunities. Sci Total Environ 625:320–335. https://doi.org/10.1016/j.scitotenv.2017.12.257

Sánchez E, Zabaleta R, Fabani MP, Rodriguez R, Mazza G (2022) Effects of the amendment with almond shell, bio-waste and almond shell-based biochar on the quality of saline-alkali soils. J Environ Manage 318:115604. https://doi.org/10.1016/j.jenvman.2022.115604

Shan Y, Li G, Bai Y, Liu H, Zhang J, Wei K, Wang Q, Cao L (2022) Effects of gypsum combined with different amounts of biochemical humic acid on soil improvement and cotton (*Gossypium hirsutum* L.) yield on saline-alkali land. Appl Ecol Environ Res 20:841–854. https://doi.org/10.15666/aeer/2001_841854

Tsai W-T, Liu S-C, Chen H-R, Chang Y-M, Tsai Y-L (2012) Textural and chemical properties of swine-manure-derived biochar pertinent to its potential use as a soil amendment. Chemosphere 89:198–203. https://doi.org/10.1016/j.chemosphere.2012.05.085

Tu YM, Yu Q, Wen RJ, Shi P, Yuan L, Ji YH, Sas G, Elfgren L (2021) Molecular dynamics simulation of coupled water and ion adsorption in the nano-pores of a realistic calcium-silicate-hydrate gel. Constr Build Mater. https://doi.org/10.1016/j.conbuildmat.2021.123961

Wang SS, Gao B, Li YC, Mosa A, Zimmerman AR, Ma LQ, Harris WG, Migliaccio KW (2015) Manganese oxide-modified biochars: preparation, characterization, and sorption of arsenate and lead. Bioresour Technol 181:13–17. https://doi.org/10.1016/j.biortech.2015.01.044

Wang PJ, Liu Q, Fan SL, Wang J, Mu SG, Zhu CB (2023) Combined application of desulfurization gypsum and biochar for improving saline-alkali soils: a strategy to improve newly reclaimed cropland in coastal mudflats. Land 12:1717. https://doi.org/10.3390/land12091717

Wang K, Wang S, Zhang X, Wang W, Wang X, Kong F, Xi M (2024a) The amelioration and improvement effects of modified biochar derived from *Spartina alterniflora* on coastal wetland soil and

Suaeda salsa growth. Environ Res 240:117426. https://doi.org/10.1016/j.envres.2023.117426

Wang M, Zhu Y, Yue C, Ge H, Yan J, Yang Y, Quan G (2024b) Preparation of a novel magnetic calcium-based biochar for arsenic removal: behavior and dominant mechanism. Sep Purif Technol 336:126384. https://doi.org/10.1016/j.seppur.2024b.126384

Wang Q, Xiao Y, Qi J, Wei H, Zhao J, Lei X, Yang D, Huang Y, Gao P (2024c) A novel strategy for preparing porous Fe/Ca-loaded biochar transformed from municipal sludge towards phosphate removal. J Water Process Eng 66:106109. https://doi.org/10.1016/j.jwpe.2024c.106109

Wu ZY, Chen XX, Yuan BL, Fu ML (2020) A facile foaming-polymerization strategy to prepare 3D MnO_2 modified biochar-based porous hydrogels for efficient removal of Cd(II) and Pb(II). Chemosphere 239:124745. https://doi.org/10.1016/j.chemosphere.2019.124745

Wu LL, Ren LP, Li J, Li X, Yang SM, Song YZ, Li XP (2022) Novel maricultural-solid-waste derived biochar for removing eutrophic nutrients and enrofloxacin: property, mechanism, and application assessment. J Hazard Mater 427:128147. https://doi.org/10.1016/j.jhazmat.2021.128147

Wu W, Chai HX, Gao PL, Gao PH, Zhang X, Li MZ, Guo XL, Lv QX (2024) Effect of biochar addition on water-salt distribution and growth of winter wheat in coastal saline-alkali soils under brackish water irrigation. Soil Use Manage. https://doi.org/10.1111/sum.13028

Xiang SY, Zhou QW, Jin MQ, Fu L, Wu WH (2024a) Preparation of biochar-supported nanoscale zero-valent iron (nZVI@ BC) and its adsorption and degradation of Chlortetracycline in water and soil. Revista Matéria 29. https://doi.org/10.1590/1517-7076-RMAT-2024-0425

Xiang X, Li X, Yang T, Cao J, Yang Z (2024b) A novel FeCa composite modified biochar prepared for enhanced Cd adsorption: experimental, DFT calculation and mechanism unveiling. J Water Process Eng 68:106565. https://doi.org/10.1016/j.jwpe.2024b.106565

Xu X, Wang JH, Tang YM, Cui XD, Hou DB, Jia HJ, Wang SB, Guo L, Wang JH, Lin AJ (2023) Mitigating soil salinity stress with titanium gypsum and biochar composite materials: improvement effects and mechanism. Chemosphere 321:138127. https://doi.org/10.1016/j.chemosphere.2023.138127

Xue Y, Kamali M, Aminabhavi TM, Appels L, Dewil R (2024) Tailoring the surface functional groups of biochar for enhanced adsorption and degradation of pharmaceutically active compounds. Chem Eng J 491:152037. https://doi.org/10.1016/j.cej.2024.152037

Yang G, Zhao H, Chen Q, Yu X, Li Z, Liu K, Zhang M, Liu Z (2020) Potassium chloride-modified urea phosphate with response surface optimization and its application effect on maize in saline-alkali soil. ACS Omega 5:17255–17265. https://doi.org/10.1021/acsomega.0c01428

Yang K, Jing W, Wang J, Zhang K, Li Y, Xia M, Zhang K, Mao J (2024) Structure–activity mechanism of sodium ion adsorption and release behaviors in biochar. Agriculture 14:1246. https://doi.org/10.3390/agriculture14081246

Yao YX (2024) Remediation of Cd(II) contamination in aqueous solution by modified sludge biochar with molten salt-assisted pyrolysis. Desalin Water Treat 317:100048. https://doi.org/10.1016/j.dwt.2024.100048

Yoon K, Cho DW, Tsang DCW, Bolan N, Rinklebe J, Song H (2017) Fabrication of engineered biochar from paper mill sludge and its application into removal of arsenic and cadmium in acidic water. Bioresour Technol 246:69–75. https://doi.org/10.1016/j.biortech.2017.07.020

Yu-yan Z, Ze-yu Z, Xiao-dan T, Li-bin Z, Xu-yang L, Ji-long L (2020) Analysis of high content water-soluble salt cation in saline-alkali soil by X-ray fluorescence spectrometry. Spectrosc Spect Anal 40:1467–1472. https://doi.org/10.1016/j.cej.2021.134441

Yuan Y, Liu Q, Zheng H, Li M, Liu Y, Wang X, Peng Y, Luo X, Li F, Li X, Xing B (2023) Biochar as a sustainable tool for improving the health of salt-affected soils. Soil & Environmental Health 1:100033. https://doi.org/10.1016/j.seh.2023.100033

Zeng Y, Li T, Ding Y, Fang G, Wang X, Ye B, Ge L, Gao J, Wang Y, Zhou D (2022) Biochar-supported nano-scale zerovalent iron activated persulfate for remediation of aromatic hydrocarbon-contaminated soil: an in-situ pilot-scale study. Biochar 4:64. https://doi.org/10.1007/s42773-022-00188-5

Zhang G, Zhang L, Shi Z, Yang Y, Liu J (2025) Microbial nutrient limitation and carbon use efficiency in saline-alkali soil amended with biochar: insights from ecoenzymatic C:N:P stoichiometry. Biochar 7:68. https://doi.org/10.1007/s42773-025-00458-y

Zhang JF, Zhang J (2020) Forestry Ecological Engineering in Coastal Saline-Alkali Soils. Study of Ecological Engineering of Human Settlements. pp 93–129

Zhang H, Shao J, Zhang S, Zhang X, Chen H (2020a) Effect of phosphorus-modified biochars on immobilization of Cu (II), Cd (II), and As (V) in paddy soil. J Hazard Mater 390:121349. https://doi.org/10.1016/j.jhazmat.2019.121349

Zhang Y, Yang J, Yao R, Wang X, Xie W (2020b) Short-term effects of biochar and gypsum on soil hydraulic properties and sodicity in a saline-alkali soil. Pedosphere 30:694–702. https://doi.org/10.1016/S1002-0160(18)60051-7

Zhang P, Bing X, Jiao L, Xiao H, Li BX, Sun HW (2022) Amelioration effects of coastal saline-alkali soil by ball-milled red phosphorus-loaded biochar. Chem Eng J 431:133904. https://doi.org/10.1016/j.cej.2021.133904

Zhang Y, Huang M, Ren H, Shi Y, Qian S, Wang Y, Zhang J, Müller C, Li S, Sardans J, Peñuelas J, Zou J (2024a) Nitrous oxide emissions in Fe-modified biochar amended paddy soil are controlled by autotrophic nitrification. Geoderma 446:116917. https://doi.org/10.1016/j.geoderma.2024a.116917

Zhang Y, Yao M, Zhai Y, Li GK (2024b) Effect of lithium slag application on saline–alkali soil amelioration and vegetable growth. Sustainability 16:3428. https://doi.org/10.3390/su16083428

Zhao YG, Wang SJ, Li Y, Liu J, Zhuo YQ, Chen HX, Wang J, Xu LZ, Sun ZT (2018) Extensive reclamation of saline-sodic soils with flue gas desulfurization gypsum on the Songnen Plain, Northeast China. Geoderma 321:52–60. https://doi.org/10.1016/j.geoderma.2018.01.033

Zhao Y, Wang S, Li Y, Zhuo Y, Liu J (2019) Effects of straw layer and flue gas desulfurization gypsum treatments on soil salinity and sodicity in relation to sunflower yield. Geoderma 352:13–21. https://doi.org/10.1016/j.geoderma.2019.06.004

Zhao W, Zhou Q, Tian Z, Cui Y, Liang Y, Wang H (2020a) Apply Biochar to ameliorate soda saline-alkali land, improve soil function and increase corn nutrient availability in the Songnen plain. Sci Total Environ 722:137428. https://doi.org/10.1016/j.scitotenv.2020.137428

Zhao W, Zhou Q, Tian ZZ, Cui YT, Liang Y, Wang HY (2020b) Apply Biochar to ameliorate soda saline-alkali land, improve soil function and increase corn nutrient availability in the Songnen plain. Sci Total Environ 722. https://doi.org/10.1016/j.scitotenv.2020.137428

Zhao W, Wang S, Tang L, Xiao J, Chen G (2025) Combined application of humic acid and attapulgite improves physical structure and nutrients in coastal saline-alkali soils. Land Degrad Dev 36:4415–4424. https://doi.org/10.1002/ldr.5643

Zhou W, Li S, Zou R, Sun X (2024) Effect of coal fly ash and green waste compost on salt ions leaching in coastal saline soils. Pol J Environ Stud 33:5497–5505. https://doi.org/10.15244/pjoes/182905

Zhou Y, Liu W, Chen D, Liu B, Lu P, Zhang Y (2025) Simultaneous remediation of As(V), Cd(II) and Pb(II) in aqueous solution and soil using Fe/Ca-modified biochar. Waste Manag Res 43:1206–1218. https://doi.org/10.1177/0734242x241307521

Zhuo SN, Dai TC, Ren HY, Liu BF (2022) Simultaneous adsorption of phosphate and tetracycline by calcium modified corn stover biochar: performance and mechanism. Bioresour Technol 359:127477. https://doi.org/10.1016/j.biortech.2022.127477